

Quantum Monte Carlo Method without Hubbard-Stratonovich Transformation for Many-body Systems

J. Wang^a, W. Pan^a and D. Y. Sun^{a,b*}

^a*Department of Physics, East China Normal University, 200241 Shanghai, China*

^b*Shanghai Qi Zhi Institute, Shanghai 200030, China*

Abstract

By precisely writing down the matrix element of the local Boltzmann operator ($e^{-\tau h}$, where h is the paired operator formed by two interacting terms conjugate to each other), we have proposed a new path integral formulation for quantum field theory and developed a corresponding Monte Carlo algorithm. Our formula presents remarkable outcomes such that: 1) the Hubbard–Stratonovich transformation is not necessary, and the auxiliary field is no longer needed, which can improve the computational efficiency. 2) The new formula improves the accuracy of the Suzuki–Trotter decomposition. Our method also provides a potential theoretical framework for analyzing and solving the fermion sign problem. As an example, we studied the one-dimensional half-filled Hubbard model at a finite temperature. The obtained results were in excellent agreement with the known solutions. The new formula and Monte Carlo algorithm could be used in various studies.

*Corresponding author.

E-mail address: dysun@phy.ecnu.edu.cn (D.-Y. Sun).

I. Introduction

Strongly correlated quantum many-body (SCQMB) systems possess a rich physical phenomenon, making them an essential topic in condensed matter physics. To overcome an exponentially increasing number of dimensions of the Hilbert space, as well as the intrinsically strong correlation of SCQMB systems, scientists have strongly advocated for efficient and accurate numerical methods.¹⁻⁶ Over the last 50 years, several numerical methods have been proposed, such as the exact diagonalization (ED) method,⁷ the density matrix renormalization group (DMRG) method,⁸⁻¹⁰ as well as various quantum Monte Carlo (QMC) methods.¹¹⁻¹³ These numerical methods have played an important role in improving the understanding of SCQMB systems over the past few decades.

In ED methods, the Hamiltonian matrix of systems is directly diagonalized using advanced mathematical techniques, but they are limited to relatively small systems. The DMRG method shares some similarities with the ED methods but it can handle larger systems, making it a more effective method for low-dimensional systems. Some examples of commonly used QMC methods include determinant QMC (DQMC),^{11,14,15} auxiliary field QMC (AFQMC),^{12,16,17} and diagrammatic MC (DiagMC).^{13,18} Recently, we developed a new method to directly calculate the ground state properties of elements of the Hamiltonian matrix, for a class of special systems.^{19,20}

The AFQMC method can be considered to be a typical example of the DQMC method. In both DQMC and AFQMC methods, the quartic fermion operators are decomposed into a quadratic form by performing the Hubbard–Stratonovich transformation.²¹⁻²³ For the DQMC method¹¹, a number of important advancements^{24,25} and improved algorithms have been developed to expedite the simulations.¹⁴ The DQMC method has been used to determine physical properties at zero^{6,26,27} and finite temperatures.^{26,28} The typical AFQMC method is a projection technique in which the operator $e^{-\beta H}$ continuously acts on a trial wave function; accordingly, the ground state properties^{12,17,24,27} can be evaluated. To avoid the fermion sign problem or phase problem, AFQMC is usually implemented by an advanced restriction on the sample

paths,²⁹ and recently, the AFQMC has additionally been developed for finite temperatures.^{16,30-32} DiagMC¹³ combines the MC technique with Feynman diagrams of the perturbative expansion to calculate physical quantities,^{18,33-37} and several generations³⁸⁻⁴¹ and improvements^{34,37,38,42,43} of this method have been developed based on the original DiagMC. For a more comprehensive introduction to various numerical methods, refer to review articles, such as those in Ref.^{2,3}

To further reduce the gap between the experimental studies and QMC calculations, more efficient numerical methods are needed to meet the current demands for studying SCQMB systems. In addition to the main bottleneck arising from the fermion sign problem, efficient numerical methods are still rare when considering the case of finite temperatures. Thus, there is an urgent need to either develop new numerical methods or optimize known ones.

In this paper, we propose a novel QMC method by introducing a new representation of the path integral formula in quantum field theory. This method can be used to calculate various properties of a system at finite temperatures. The new formulation does not require any additional transformations or auxiliary fields, and therefore the calculation time can be significantly reduced. The results of the test calculation on the one-dimensional Hubbard model are in excellent agreement with the known, exact values.^{44,45}

II. Proposed Formula

To illustrate our method, we chose the simple and representative Hubbard model as an example. It is worth noting that our method can be directly extended to any model or Hamiltonian. The Hamiltonian of the Hubbard model is as follows:

$$H = - \sum_{i,j,\sigma} t (c_{i\sigma}^\dagger c_{j\sigma} + H.c.) + U \sum_i n_{i\uparrow} n_{i\downarrow}, \quad (1)$$

where $c_{i\sigma}^\dagger$ ($c_{i\sigma}$) denotes the creation (annihilation) of an electron with spin $\sigma = \uparrow, \downarrow$ at the i -th lattice site. The first term on the right-hand side of Eq. (1) represents the one-body term, which accounts for the hopping of electrons between different sites, and $t > 0$ is the overlap integral. The second term is the two-body on-site Coulomb

interaction, where U represents the interaction strength, and $n_{i\sigma} = c_{i\sigma}^\dagger c_{i\sigma}$ is the number operator for spin σ at the i -th site. For convenience, the spin index is omitted in the following description; yet it is included later on to prevent confusion.

One of the key aspects of our method is to combine each single term in the Hamiltonian and its Hermite conjugate into pairs, namely $h_{ij} = -t(c_i^\dagger c_j + c_j^\dagger c_i)$. Clearly h_{ij} is therefore a Hermitian operator. In the case of a general Hamiltonian, h_{ij} could be the pair of a quartic fermion operator and its Hermitian conjugation. The purpose of this combination is to make h_{ij} a Hermitian operator.

A many-body wave function (WF) in the occupation number representation is labeled as $|ijK\rangle$. Here, the occupancy of the i -th and j -th sites is explicitly given, while the occupancy of the rest of the sites is represented by K . For the i -th and j -th sites, the occupation has four cases, which are labeled as $|i\bar{j}K\rangle, |\bar{i}jK\rangle, |ijK\rangle,$ and $|\bar{i}\bar{j}K\rangle$. Here, $\bar{i}(\bar{j})$ indicates that there is no electron occupying the i -th (j -th) site, while i (j) indicates an electron occupying the i -th (j -th) site.

It is easy to prove that h_{ij} has only two eigenstates with non-zero eigenvalues:

$$|\varphi_{ij}\rangle_+ = \frac{1}{\sqrt{2}}(|i\bar{j}K\rangle + |\bar{i}jK\rangle) ; |\varphi_{ij}\rangle_- = \frac{1}{\sqrt{2}}(|i\bar{j}K\rangle - |\bar{i}jK\rangle),$$

where the eigenvalues are equal to $-\theta t$ and θt , respectively. θ is the sign produced by the particle exchange as h_{ij} acts on $|i\bar{j}K\rangle$. When an even number of exchanges occur, $\theta = 1$, otherwise, $\theta = -1$. The remaining WFs orthogonal to $|\varphi_{ij}\rangle_+$ and $|\varphi_{ij}\rangle_-$ are also the eigenstates of h_{ij} ; however, the corresponding eigenvalues are zero.

It is easy to demonstrate that in the particle number representation, the non-zero matrix elements of the local Boltzmann operator (LBO), $e^{-\tau h_{ij}}$, where τ can be any number, are only present in the following cases:

$$\langle i\bar{j}K | e^{-\tau h_{ij}} | \bar{i}jK' \rangle = \langle \bar{i}jK | e^{-\tau h_{ij}} | i\bar{j}K' \rangle = \frac{1}{2} \delta_{K,K'} (e^{\theta\tau t} - e^{-\theta\tau t}), \quad (2.1)$$

$$\langle i\bar{j}K | e^{-\tau h_{ij}} | i\bar{j}K' \rangle = \langle \bar{i}jK | e^{-\tau h_{ij}} | \bar{i}jK' \rangle = \frac{1}{2} \delta_{K,K'} (e^{\theta\tau t} + e^{-\theta\tau t}), \quad (2.2)$$

$$\langle ijK | e^{-\tau h_{ij}} | ijK' \rangle = \langle \bar{i}\bar{j}K | e^{-\tau h_{ij}} | \bar{i}\bar{j}K' \rangle = \delta_{K,K'}, \quad (2.3)$$

where the remaining matrix elements of $e^{-\tau h_{ij}}$ are equal to zero. Since the operator $e^{-\tau U n_{i\uparrow} n_{i\downarrow}}$ is diagonal, the non-zero matrix element reads:

$$\langle i_{\uparrow} i_{\downarrow} K | e^{-\tau U n_{i\uparrow} n_{i\downarrow}} | i_{\uparrow} i_{\downarrow} K' \rangle = \delta_{K, K'} e^{-\tau U}. \quad (2.4)$$

Since $t > 0$, the matrix elements in Eqs. (2.2 – 2.3) are always positive, regardless of the value of θ . The matrix element in Eq. (2.1) is negative if θ is negative, otherwise, it is positive.

The partition function of a quantum many-body system is expressed as $Z = \text{Tr}[e^{-\beta H}]$, where β is the inverse temperature (or imaginary time). According to the standard path integral formula, the imaginary time (β) is divided into m time-slices, where the partition function then becomes $Z = \text{Tr}[(e^{-\tau H})^m]$, with the time step $\tau = \beta/m$. Using the Suzuki–Trotter decomposition,²¹⁻²³ the operator $e^{-\tau H}$ can be further decomposed as

$$e^{-\tau H} = \prod_{ij} e^{-\tau h_{ij}} \prod_i e^{-\tau U n_{i\uparrow} n_{i\downarrow}}.$$

Finally, the partition function reads:

$$Z = \text{Tr} \prod_{ij} e^{-\tau h_{ij}} \prod_i e^{-\tau U n_{i\uparrow} n_{i\downarrow}} \dots \prod_{ij} e^{-\tau h_{ij}} \prod_i e^{-\tau U n_{i\uparrow} n_{i\downarrow}} = \sum_{\omega} \rho(\omega), \quad (3)$$

where ω refers to a closed path (a WF sequence) in the wavefunction space, and $\rho(\omega)$ is the associated Boltzmann weight. To calculate the partition function, complete orthogonal sets are inserted between the two LBOs. For the purpose of this discussion, we number each LBO ($e^{-\tau h}$, $h = h_{ij}$ or $U n_{i\uparrow} n_{i\downarrow}$) in Eq. (3) from right to left as, 1st, 2nd, ... i -th LBO. The WF following the k -th LBO is then denoted by the k -th WF. A closed WF sequence is labeled as $\omega = \{\dots |s\rangle \dots\}$, where $|s\rangle$ is the s -th WF.

Because only the matrix elements in Eqs. (2.1 – 2.4) are non-zero, for any closed path, the Boltzmann weight has the following form:

$$\rho(\omega) = \left(\frac{1}{2}(e^{\tau t \theta} + e^{-\tau t \theta})\right)^{n_+} \left(\frac{1}{2}(e^{\tau t \theta} - e^{-\tau t \theta})\right)^{n_-} (e^{-\tau U})^{n_0}, \quad (4)$$

where n_-, n_+, n_0 correspond to the number of occurrences of the matrix elements in Eq. (2.1, 2.2, and 2.4) for a closed path ω , respectively.

Eq. (4) is the key formula of our newly proposed method, which represents the

weighting of a path in the path integral formula. Eq. (4) shows that our method has several novel features: 1) The new formula does not include the Hubbard–Stratonovich transformation, and thus it does not require the auxiliary field; 2) The Fermion sign problem is solely determined by $\left(\frac{1}{2}(e^{\tau t\theta} - e^{-\tau t\theta})\right)^{n_-}$, so that if $\theta > 0$, the fermion sign problem will be automatically eliminated within our new formulation; 3) Our formula improves the accuracy of Suzuki–Trotter decomposition. The error caused by the Suzuki–Trotter decomposition mainly arises from the commutators between an operator and its Hermite conjugate. However, in our proposed formulation, the operator and its Hermite conjugate only appear in pairs. Additionally, for the Hubbard Hamiltonian, the operators $c_i^\dagger c_j$ and $c_j^\dagger c_i$ always appear in pairs in $e^{-\tau h_{ij}}$.

III. New Monte Carlo Algorithm

To implement the new formula presented in Eq. (4) into the QMC simulations, we subsequently developed a set of efficient algorithms. Although it is easy to calculate the weighting of each path, it is relatively difficult to find a path with a non-zero weight, due to the fact that the weight of most paths is zero.

The choice of each state is very significant for obtaining a path with a non-zero weighting. Here, we design an algorithm similar to the multiple time threading algorithm.⁴⁶ Specifically, we first randomly select a wave function from the last MC WF sequence, $\omega = \{\dots |s\rangle \dots\}$, in which $|s\rangle$ refers to the s -th WF. Then, $|s\rangle$ is scattered by the s -th LBO, and a new WF $|s+1\rangle'$ is defined and obtained such that $|s+1\rangle' = e^{-\tau' h_s} |s\rangle$, where $h_s = h_{ij}$ or $Un_{i\uparrow}n_{i\downarrow}$. Next, $|s+1\rangle'$ is scattered by the $(s+1)$ -th LBO, and the $(s+1)$ -th WF $|s+2\rangle'$, i.e., $|s+2\rangle' = e^{-\tau' h_s} |s+1\rangle'$ is generated. It is worth noting that the value of τ' may be different from that of τ presented in Eq. (4), and the selection of this was performed to improve the efficiency of the QMC simulations. This process continues until all the LBOs are cycled in the same sequence as in Eq. (3).

In the above scattering process, the progression of $e^{-\tau' Un_{i\uparrow}n_{i\downarrow}}$ does not produce

any bifurcation because it is diagonal. However, for the operator $e^{-\tau' h_{ij}}$, if one of the i -th or j -th sites is occupied and the other is empty, the scattering will be bifurcated. One side of the bifurcation corresponds to Eq. (2.1), in which the occupancy of the i -th and j -th sites is exchanged before and after scattering, while the other path corresponds to Eq. (2.2), in which the wave function is unchanged before and after scattering. For the bifurcation, we use a similar heat-bath algorithm⁴⁷ to select the new path, namely, the path following Eq. (2.1) with the probability of $\rho_{HB}(-) = \frac{(e^{\theta\tau t} - e^{-\theta\tau t})}{2e^{-\theta\tau\epsilon}}$, and the other path following Eq. (2.2) with the probability of $\rho_{HB}(+) = \frac{(e^{\theta\tau t} + e^{-\theta\tau t})}{2e^{-\theta\tau\epsilon}}$.

A scattering path defined as $\omega' = \{|1\rangle' \dots |s\rangle' \dots\}$ has now successfully been obtained. With the exception of the case in which $|s\rangle = |s\rangle'$, the scattering path may have multiple intersections with the old one ($\omega = \{\dots |s\rangle \dots\}$). The intersection means that the WF is identical in both the new and old paths and is in the same position in Eq. (3). We randomly choose the scattering path between any two intersection points to replace the old path, thereby representing a new QMC path. It should be noted that the probability of finding a new path using this method is remarkably high, i.e., close to 100 %.

The acceptance rate of the new path is determined by the ratio of two factors, namely $ccpt = \frac{\rho(\omega_{new})}{\rho(\omega_{old})} \cdot \frac{1}{\rho_{HB}(\pm)}$, where $\frac{\rho(\omega_{new})}{\rho(\omega_{old})}$ is the ratio of the weights of the new to old paths. $\rho_{HB}(\pm) = \frac{(e^{-\theta\tau\epsilon} \pm e^{\theta\tau\epsilon})}{2e^{-\theta\tau\epsilon}}$ is the additional weight attached to the heat-bath sampling, which should be deducted from the acceptance rate. If the change is accepted, the updated WFs are implemented. Otherwise, the unchanged WFs are implemented.

There are several techniques to preform our QMC simulations: 1) The initial WF sequence is simply made up of a randomly chosen WF; 2) For most simulations, the total number of QMC steps is approximately 10^7 , where the first third of the steps are used to equilibrate the system and the remaining two thirds of the steps are used to calculate the physical properties; 3) The value of τ' has no effect on the final results, but can speed up the convergence. For the one-dimensional Hubbard model, the effect of τ' was insignificant. However, it is worth mentioning that, in general, a smaller

value of τ' ($\tau' < \tau$) is favorable for a higher efficiency.

IV. Tests on Hubbard Model

The Hubbard model can appropriately describe many favorable and interesting characteristics of correlated electronic systems. Many studies based on the Hubbard model have been carried out to investigate the metal-insulator transition, superconductivity, and magnetic properties caused by electronic correlation. Lieb and Wu⁴⁸ obtained the exact solution of the ground state for the half-filled one-dimensional Hubbard model. In the last few decades, various theoretical calculations have been carried out to study the one-dimensional Hubbard model. However, few studies have been conducted using this model at finite temperatures.^{44,45,49-54}

To illustrate the reliability of our new formula and the new QMC algorithm, we studied the one-dimensional Hubbard model at a finite temperature. In all calculations, t was taken to have units of energy and was set to $t = 1.0$. The strength of the interaction was also investigated for $U = 4t$ and $8t$. In typical QMC simulations, the Boltzmann weight is represented by a determinant. The sign of the determinant is not necessarily positive for fermions. Thus, for particular special cases, the sign problem is not encountered.^{26,55} By choosing appropriate boundary conditions (periodic or antiperiodic) for systems of different sites, the sign problem can be avoided when using our formulation.

The energy, double occupancy, local magnetic moments, and spin correlation functions were calculated in the temperature range of 0.05 to 4.0. According to thermodynamics, the energy of systems can be calculated as $E = -\frac{1}{Z} \frac{\partial Z}{\partial \beta}$. The double occupancy, denoting the probability of two electrons occupying one site, is written as $O_d = \langle n_{i\uparrow} n_{i\downarrow} \rangle$. $L_0 = \frac{3}{N} \sum_i \langle (S_i^z)^2 \rangle$ is the local magnetic moment, where $S_i^z = \frac{1}{2} \sum_i (n_{i\uparrow} - n_{i\downarrow})$ denotes the z -component spin operator at the i -th site. The nearest-neighbor and next-nearest-neighbor spin correlation functions are defined as $L_1 = \frac{1}{N} \langle S_i^z S_{i+1}^z \rangle$ and $L_2 = \frac{1}{N} \langle S_i^z S_{i+2}^z \rangle$.

The convergence test on τ is shown in Fig. 1, where the upper and lower panels present the data for $U = 4$ and 8, respectively. It can be seen that, with an increase in the number of time slices m , τ decreases and the energy converges quickly. At $m = 80$, corresponding to $\tau = 0.05$, the QMC results approach the exact, known value with a difference of approximately 1 % and 5 % for $U = 4$ and 8, respectively. Owing to the intrinsic characteristics of the path integral formula, the exact value can be obtained only when τ approaches zero. Fortunately, as long as τ is sufficiently small, the path integral within the QMC method provides reasonable results. In the following QMC simulations, τ was fixed to have a value of 0.05.

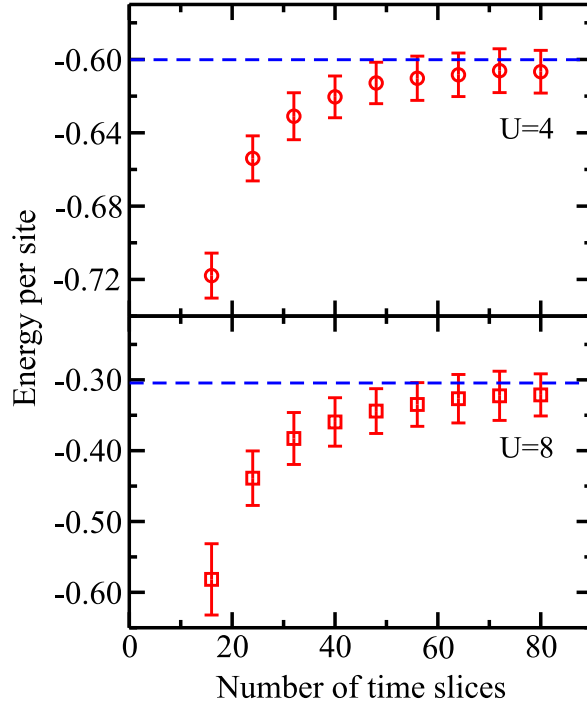


FIG. 1. Energy per site as a function of the number of time slices (m) for $U = 4$ (upper panel) and $U = 8$ (lower panel), at a temperature of 0.25. The symbol and dashed lines represent the QMC data and the exact value, respectively. At $m = 80$, i.e., $\tau = 0.05$, the QMC results are convergent.

Fig. 2 depicts the energy, double occupancy, and specific heat via temperature for $U = 4$ (left panel) and 8 (right panel). The energy calculated by the QMC simulation is in excellent agreement with the exact value for the entire range of temperatures within

the error bar (upper panel of Fig. 2). Compared to $U = 4$, for $U = 8$, there is an evident plateau in the temperature range of 1.0 to 2.0. The plateau reflects the fact that the on-site Coulomb interaction has a strong effect in suppressing the occurrence of double occupancy. The change in double occupancy with temperature supports this conclusion.

From the middle panel of Fig. 2, it can be seen that, from the high temperature to the lower temperature, the double occupancy first decreases and then increases for $U = 4$ and $U = 8$. Although the double occupancy increases at low temperatures, the total energy is further reduced with a corresponding decrease in temperature. This reflects the fact that a small increase of the delocalization doublon further decreases the total energy.^{44,56} For $U = 4$, the increase in the double occupancy is more evident than when $U = 8$ at lower temperatures. At a fixed temperature, the double occupancy is larger than it is for $U = 8$, demonstrating how the on-site interaction has a noticeable impact on the formation of the double occupations.

The specific heat as a function of temperature is shown in the lower panel of Fig. 2. To calculate the specific heat, the exponential fitting method⁵⁷⁻⁵⁹ is adopted with the fitting form of $E(T) = E(0) + \sum_{n=1}^M c_n e^{\frac{-n\alpha}{T}}$, where $E(0)$, c_n and α are the fitting parameters. In this study, the value of M was 8. From Fig. 2, it can be seen that there are two obvious peaks in the specific heat when $U = 8$. Specifically, there is a narrow peak at low temperatures and a broad peak at high temperatures. In contrast, for $U = 4$, the two peaks become much closer and begin to merge together. The structure of the obtained specific heat peak is consistent with previous findings.^{44,51,52} It is believed that this feature in the specific heat is associated with the spin-wave excitations at low temperatures and the single-particle excitations at high temperatures. Thus, spin fluctuations and charge fluctuations are dominant at low and high temperatures, respectively, which can be highlighted by the correlation functions (see below).

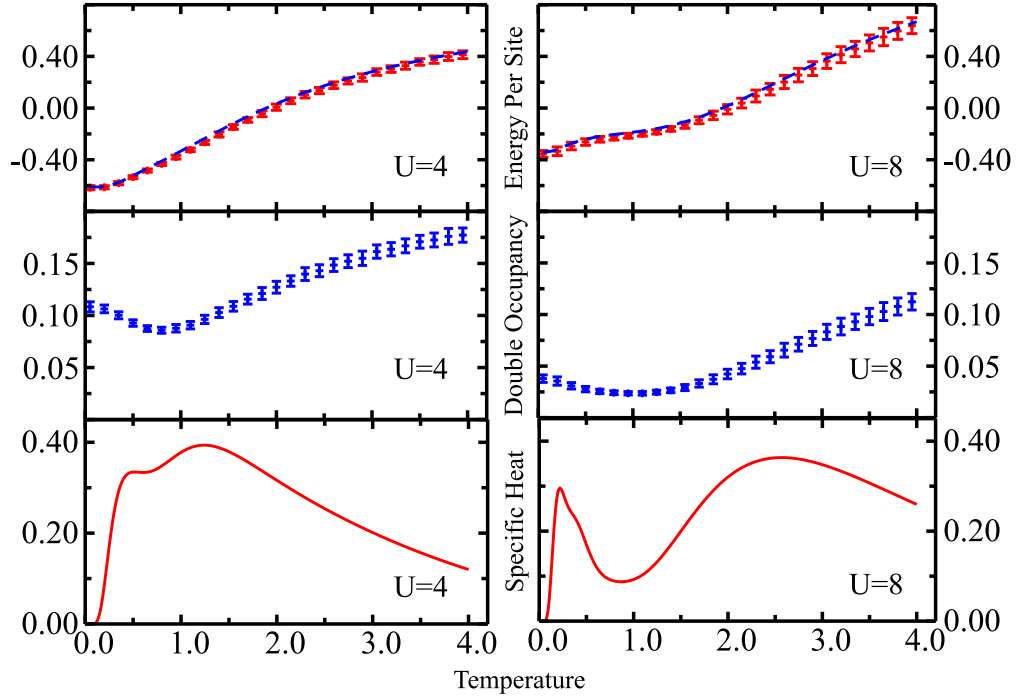


FIG. 2. Energy (upper panels), double occupancy (middle panels), and specific heat (bottom panels) as a function of temperature for $U = 4$ (left panels) and $U = 8$ (right panels). The QMC results (symbols) are in excellent agreement with the exact value (dashed lines) across the entire range of temperatures.

Fig. 3 shows the local moment ($L_{\alpha=0}$) and spin correlation functions ($L_{\alpha=1,2}$) as a function of temperature for $U = 4$ (left panel) and $U = 8$ (right panel). With an increasing temperature, L_0 reaches its maximum at a certain temperature and then gradually decreases. The maximum value obtained for L_0 indicates that at this temperature, the degree of localization of electrons is the largest. The degree of delocalization of electrons reflects the formation of doublons; therefore, the trends of local moment and double occupancy are reversed, as shown in the upper panels of Fig. 3 and the middle panels of Fig. 2. From the lower panel of Fig. 3, one can see that L_1 is less than zero, which indicates an antiferromagnetic order at a finite temperature, which leads to the emergence of a specific heat peak at a lower temperature. As the temperature increases, L_1 decreases and tends to zero, reflecting a weakened antiferromagnetic order; this is in agreement with the exact results. In contrast, L_2 is

greater than zero and gradually reduces to zero with a corresponding increase in temperature. In general, the trends of L_1 and L_2 are consistent with the results of Shiba.^{44,45}

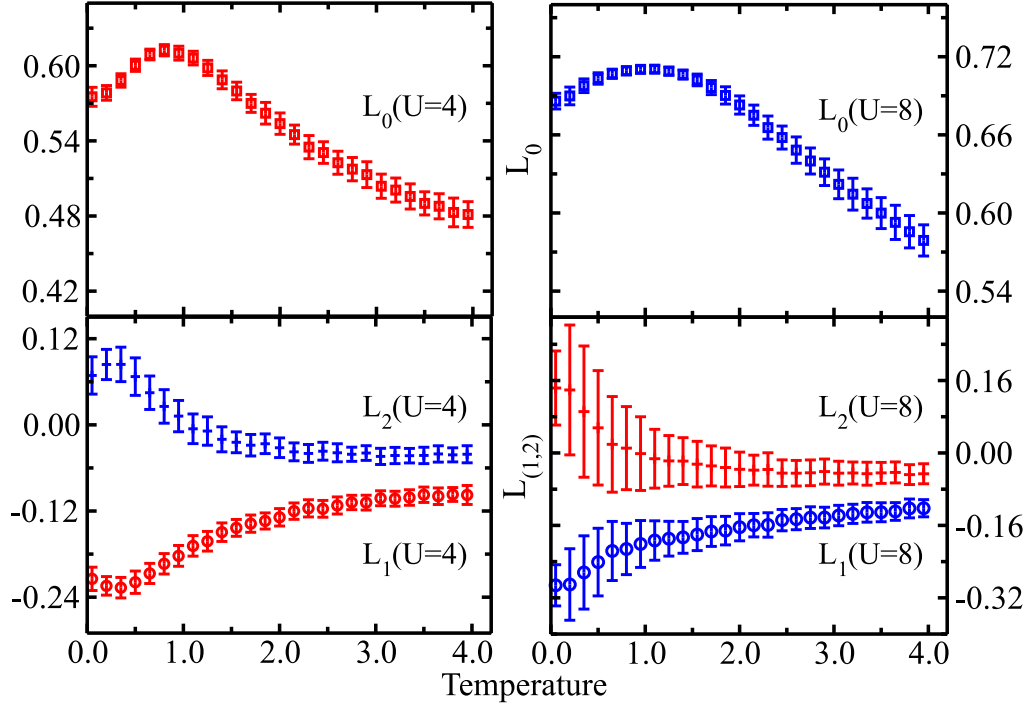


FIG. 3. Local moment ($L_{\alpha=0}$) and correlation functions ($L_{\alpha=1,2}$) as a function of temperature for $U = 4$ (left panel) and $U = 8$ (right panel). L_0 , L_1 , and L_2 represent the local magnetic moment, the nearest-neighbor spin correlation, and the next-nearest-neighbor spin correlation, respectively.

V. Summary

We have proposed a new path integral formula in field theory and a corresponding new quantum Monte Carlo algorithm, which can improve the accuracy and efficiency of Monte Carlo calculations. The new formula provides an alternative way to study strongly correlated systems at finite temperatures. As an example, we calculated the thermodynamic quantities and correlation functions of the one-dimensional Hubbard model at a finite temperature. Our results are in excellent agreement with the exact, known values, confirming the reliability of our method. Our proposed formula could

be combined with other Monte Carlo technique, and our new program could also be incorporated into other Monte Carlo methods. We believe that our approach could be widely used in future.

Acknowledgements: Project supported by the National Natural Science Foundation of China (Grant No. 11874148). The computations were supported by ECNU Public Platform for Innovation.

References:

- 1 L. Pollet, Rep. Prog. Phys **75**, 094501 (2012).
- 2 J. P. F. LeBlanc *et al.*, Phys. Rev. X **5**, 28, 041041 (2015).
- 3 T. Schäfer *et al.*, Phys. Rev. X **11**, 011058 (2021).
- 4 B.-B. Chen, C. Chen, Z. Chen, J. Cui, Y. Zhai, A. Weichselbaum, J. von Delft, Z. Y. Meng, and W. Li, Phys. Rev. B **103**, L041107 (2021).
- 5 J. Zaanen, Science **319**, 1205 (2008).
- 6 E. Y. Loh, J. E. Gubernatis, R. T. Scalettar, S. R. White, D. J. Scalapino, and R. L. Sugar, Phys. Rev. B **41**, 9301 (1990).
- 7 E. Dagotto, Rev. Mod. Phys. **66**, 763 (1994).
- 8 S. R. White, Phys. Rev. Lett. **69**, 2863 (1992).
- 9 S. R. White, Phys. Rev. B **48**, 10345 (1993).
- 10 T. Xiang, Phys. Rev. B **53**, R10445 (1996).
- 11 R. Blankenbecler, D. J. Scalapino, and R. L. Sugar, Phys. Rev. D **24**, 2278 (1981).
- 12 S. Sorella, S. Baroni, R. Car, and M. Parrinello, Europhys. Lett. **8**, 663 (1989).
- 13 N. V. Prokof'ev and B. V. Svistunov, Phys. Rev. Lett. **81**, 2514 (1998).
- 14 C.-C. Chang, S. Gogolenko, J. Perez, Z. Bai, and R. T. Scalettar, Philos. Mag **95**, 1260 (2015).
- 15 R. R. dos Santos, Braz. J. Phys. **33**, 36 (2003).
- 16 Z.-Y. Xiao, H. Shi, and S. Zhang, Phys. Rev. Research **3**, 013065 (2021).
- 17 G. Sugiyama and S. E. Koonin, Ann. Phys. (N.Y.) **168**, 1 (1986).
- 18 F. Šimkovic, R. Rossi, and M. Ferrero, Phys. Rev. B **102**, 195122 (2020).
- 19 W. Pan, J. Wang, and D. Sun, Sci. Rep. **10**, 3414 (2020).
- 20 W. Pan, J. Wang, and D. Sun, Phys. Lett. A **384**, 126610 (2020).
- 21 H. F. Trotter, Proc. Am. Math. Soc. **10**, 545 (1959).
- 22 M. Suzuki, Prog. Theor. Phys. **56**, 1454 (1976).
- 23 R. M. Fye, Phys. Rev. B **33**, 6271 (1986).
- 24 S. R. White, D. J. Scalapino, R. L. Sugar, E. Y. Loh, J. E. Gubernatis, and R. T. Scalettar, Phys. Rev. B **40**, 506 (1989).
- 25 F. F. Assaad and H. G. Evertz, in *Computational Many-Particle Physics* edited by H. Fehske, R. Schneider, and A. Weiße (Springer, 2008), pp. 277–356.
- 26 J. E. Hirsch, Phys. Rev. B **31**, 4403 (1985).
- 27 F. Becca and S. Sorella, in *Quantum Monte Carlo Approaches for Correlated Systems* (Cambridge University Press, 2017), pp. 214–232.
- 28 E. Y. Loh, J. E. Gubernatis, R. T. Scalettar, S. R. White, D. J. Scalapino, and R. L. Sugar, Int. J. Mod. Phys. C **16**, 1319 (2005).

- 29 S. Zhang, J. Carlson, and J. E. Gubernatis, Phys. Rev. Lett. **74**, 3652 (1995).
- 30 S. Zhang, Phys. Rev. Lett. **83**, 2777 (1999).
- 31 Y.-Y. He, M. Qin, H. Shi, Z.-Y. Lu, and S. Zhang, Phys. Rev. B **99**, 045108 (2019).
- 32 Y.-Y. He, H. Shi, and S. Zhang, Phys. Rev. Lett. **123**, 136402 (2019).
- 33 A. A. Abrikosov, L. P. Gor'kov, and I. Ye. Dzyaloshinsky, *Quantum Field Theoretical Methods in Statistical Physics* (Pergamon, Oxford, 1965).
- 34 W. Wu, M. Ferrero, A. Georges, and E. Kozik, Phys. Rev. B **96**, 041105 (2017).
- 35 R. Rossi, F. Werner, N. Prokof'ev, and B. Svistunov, Phys. Rev. B **93**, 161102 (2016).
- 36 K. Van Houcke, E. Kozik, N. Prokof'ev, and B. Svistunov, Phys. Procedia **6**, 95 (2010).
- 37 E. Kozik, K. Van Houcke, E. Gull, L. Pollet, N. Prokof'ev, B. Svistunov, and M. Troyer, Europhys. Lett. **90**, 10004 (2010).
- 38 F. Šimkovic and E. Kozik, Phys. Rev. B **100**, 121102 (2019).
- 39 A. Moutenet, W. Wu, and M. Ferrero, Phys. Rev. B **97**, 085117 (2018).
- 40 R. Rossi, arXiv:1802.04743.
- 41 R. Rossi, Phys. Rev. Lett. **119**, 045701 (2017).
- 42 F. Šimkovic, J. P. F. LeBlanc, A. J. Kim, Y. Deng, N. V. Prokof'ev, B. V. Svistunov, and E. Kozik, Phys. Rev. Lett. **124**, 017003 (2020).
- 43 A. J. Kim, F. Šimkovic, and E. Kozik, Phys. Rev. Lett. **124**, 117602 (2020).
- 44 H. Shiba and P. A. Pincus, Phys. Rev. B **5**, 1966 (1972).
- 45 H. Shiba, Prog. Theor. Phys. **48**, 2171 (1972).
- 46 E. L. Pollock and D. M. Ceperley, Phys. Rev. B **30**, 2555 (1984).
- 47 D. M. Ceperley, Rev. Mod. Phys. **67**, 279 (1995).
- 48 E. H. Lieb and F. Y. Wu, Phys. Rev. Lett. **20**, 1445 (1968).
- 49 J. C. Bonner and M. E. Fisher, Phys. Rev. **135**, A640 (1964).
- 50 M. Takahashi, Prog. Theor. Phys. **52**, 103 (1974).
- 51 J. Schulte and M. C. Böhm, Phys. Status Solidi B **199**, 59 (1997).
- 52 J. Schulte and M. C. Böhm, Phys. Rev. B **53**, 15385 (1996).
- 53 M. Takahashi, Prog. Theor. Phys. **47**, 69 (1972).
- 54 C. Yang, A. N. Kocharian, and Y. L. Chiang, Int. J. Mod. Phys. B **17**, 3354 (2003).
- 55 V. I. Iglovikov, E. Khatami, and R. T. Scalettar, Phys. Rev. B **92**, 045110 (2015).
- 56 A. Georges and W. Krauth, Phys. Rev. B **48**, 7167 (1993).
- 57 T. Paiva, C. Huscroft, A. K. McMahan, and R. T. Scalettar, J. Magn. Magn. Mater **226**, 224 (2001).
- 58 A. K. McMahan, C. Huscroft, R. T. Scalettar, and E. L. Pollock, J. Comput.-Aided Mater. Des. **5**, 131 (1998).
- 59 T. Paiva, R. T. Scalettar, C. Huscroft, and A. K. McMahan, Phys. Rev. B **63**, 125116 (2001).